The International Journal of Advanced Manufacturing Technology
https://doi.org/10.1007/s00170-024-13475-1

ORIGINAL ARTICLE

Performance evaluation of polymer-filled metal fused filament fabrication tooling for profile extrusion

Martin Kain[1] · Paolo Parenti[2] · Massimiliano Annoni[2] · Matteo Calaon[1] · David Bue Pedersen[1] · Guido Tosello[1]

Received: 6 December 2023 / Accepted: 18 March 2024

Abstract
The application of additive manufacturing (AM) for tooling in the mould and die industry brings a disruptive potential in process performance, design flexibility and product enhancements. Maturing of existing AM technologies and emerging technologies such as metal-fused filament fabrication (metal FFF) can further support the applicability of AM tooling in polymer profile extrusion. This study provides a complete characterization of metal FFF 17–4 PH stainless-steel die inserts and evaluates their applicability in a polymer extrusion process chain. The presented experimental assessment pivots on the metrological characterization of the produced inserts and the impact of the insert characteristics on the final extrudates' product. Considering a conventionally manufactured benchmark insert, produced via subtractive methods (CNC machining and electrical discharge machining), comparable results for AM tools in terms of extrudates' quality and process repeatability are presented. It was found that despite significant higher average surface parameters for AM insert tools ($Sa = 2$–9 µm vs. $Sa = 0.3$–0.9 µm for dies manufactured by machining), a much smaller difference was observed in the resulting quality of polymer extrudates' product. The roughness generation effect of polymer profile extrusion based on the different dies' internal surface roughness topography and the effect on extrudates product was evaluated. Three-dimensional average roughness *Sa* on acrylonitrile butadiene styrene extrudate surfaces obtained from conventionally machined dies was in the range of 0.3 µm. For extrudates obtained from additively manufactured dies, their *Sa* was in the rage of 0.5 µm (despite the much higher surface roughness of FFF dies compared to machined dies). The results confirm that with suitable extrudates' product requirement, it is feasible to apply metal FFF as the selected manufacturing method for tooling in polymer profile extrusion.

Keywords Additive manufacturing · Hard tooling · Extrusion · Die insert · Surface roughness

1 Introduction

During recent decades, the research, development, innovation and maturing of additive manufacturing (AM) technologies has led to a broader application of AM in industrial manufacturing [1]. The initial implementation of AM was reserved for applications concerning one-of-a-kind, complex, specialized prototyping part geometries that would have resulted in near-impossible manufacturing procedures and unreasonable costs had conventional subtractive manufacturing (SM) technologies been applied [2]. However, with an increasingly competitive AM market, new technologies are emerging, resulting in improved processes at a competitive cost [3]. Today, metal-based AM (MAM) is not reserved for one-of-a-kind parts but is more widely applicable, making large-scale testing and following application a reality.

The cost of MAM is challenging to be compared to conventional tooling because MAM provides a different level of complexity to parts, making it possible to convert entire assemblies into single parts [4, 5]. In fact, a simple adaptation of a conventional SM part assembly will likely not reduce the overall cost [3]. In order to be competitive, the AM part must be optimized for the specific AM process, just as conventional parts are optimized for their respective SM processes [5, 6]. Even after a simple design reworking to comply with design for AM, the full benefit of AM is yet to be explored. As AM allows for a completely different design process, a potential starting point could be an optimized simulation of an application or process [7]. As most simulations

✉ Guido Tosello
guto@dtu.dk

[1] Department of Civil and Mechanical Engineering, Technical University of Denmark, 2800 Kongens Lyngby, Denmark

[2] Department of Mechanical Engineering, Politecnico Di Milano, 20133 Milan, Italy

Published online: 09 April 2024

provide complex solutions which must be simplified for SM, due to manufacturing process constraints, simplifications are not necessary to the same extent with AM, potentially yielding final parts and products much closer to an ideal design. When this entire chain is considered, it will become reasonable to compare the cost of conventional SM with AM [4].

The application of MAM in the tooling process chain within the polymer industry has generated considerable progress, especially in injection moulding. When incorporating conformal cooling channels in MAM injection moulds, reducing cycle times by 30–40% is not uncommon [8, 9]. This development is supported by extensive work on multiphysics simulations, considering the influence of thermal, mechanical and fluid dynamics. Implementing complex conformal cooling channel geometries in injection moulds is entirely enabled by MAM and is increasingly applied with high-volume part production [8]. Fundamentally injection moulding is based on the cyclic extrusion of a molten polymer through a channel into a die. The overall process layout is closely related to the conceptual basis of profile extrusion. Based on the significant developments and process improvements experienced in injection moulding, implementing some of the same concepts and technologies may result in a similar disruption of the profile extrusion industry as well.

In a different yet comparable field of application, MAM for tooling has been applied in the extrusion of aluminium profiles. An example of improved hot aluminium extrusion process using additively manufactured dies has been reported where optimized conformal cooling channels for die-heating applications have had a significant impact compared to conventional dies manufactured through SM [10–12].

In comparison, the application of MAM for tooling in polymer profile extrusion is yet to experience the same progress seen within the injection moulding industry. Since the late 90 s, very little work has been published, starting with initial investigations presented by Munot et al. (1999), who applied polymer-based AM technologies for manufacturing dies for polymer extrusion [13]. More recently, Yesildag et al. (2017) published conceptual considerations for applying MAM technologies for manufacturing polymer profile extrusion dies. However, this particular study did not include implementation and experimental work [14]. A published feasibility study by some of the authors of the current publication has reported on the successful implementation of L-PBF in the tooling process chain for polymer profile extrusion with resulting extrudates comparable with that of conventionally manufactured extrusion dies [15].

The current application of MAM is generally reserved for part geometries where the external surface is accessible and can be post-processed either through SM or other post-processing. This limitation is due to the typical as-built MAM surface being significantly rougher and with complex topographical features [16]. The requirements regarding surface topography within the cavity of a mould in the polymer industry are very dependent on the expected use of the manufactured part. That said, surface roughness in the sub-micrometre range or parts with sub-millimetre surface features are now consistently achievable in polymer injection moulding. This is possible due to the resulting surface topographies originating from conventional SM processes that have been perfected and optimized for decades. Thus, when MAM parts are incorporated into an injection moulding setup, they are typically treated as blank substrates and finished using CNC milling combined with specific surface treatments to comply with widely accepted tooling industrial standards [5, 17, 18]. By implementing these hybrid tooling solutions, the free-form capabilities of MAM and the ability to manufacture internal structures (e.g. conformal cooling channels) are exploited. At the same time, the superior features of surface finish and dimension accuracy are maintained by applying SM processes [6].

The internal flow cavity of a polymer profile extrusion die is usually not readily accessible for post-processing due its depth and geometrical complexity. Therefore, the original condition of the surface after the primary shaping production technology is essential. The interaction between the polymer flow inside the MAM as-built die surface and the resulting surface roughness of the extrudate product is of interest. To the authors' knowledge, very little published work exists on the specific topic of the die internal surface topography and the resulting polymer extrudate external surface topography. Early work by Mackley et al. (1998) reports on the influence of extensional stress peak at the die exit and the influence on extrudates' surface roughness. However, it does not consider different internal die surface roughness [19]. The work by Arda et al. (2005) reported on the investigation of sharkskin extrusion instabilities and melt fracture experienced with different additives, die exit curvatures and die roughness and revolves around the melt/wall separation point and polymer stress concentration upon the die exit [20]. The manufacturing method and the internal surface topographies of the dies were not specified in this study, and the included dies had roughness in the single-digit micrometre down to the sub-micrometre range, so not in a range typically found in as-built MAM surfaces. Thus, investigating the influence of MAM surfaces in polymer profile extrusion is essential for the successful integration of MAM in the tooling process chain of profile extrusion.

As previously mentioned, preliminary published studies by the authors [21] have shown positive indications of the capability of MAM dies to manufacture extrudate products with a resulting surface roughness compliant with product requirements and comparable to products manufactured using conventional tools. These investigations were conducted using L-PBF as the choice of MAM technology.

L-PBF has many advantages, such as high resolution, relatively low MAM surface roughness, high availability of different materials and many different machine providers [19]. However, the equipment and manufacturing cost is high, and the requirements for powder handling and cleaning facilities make it complex to set up a manufacturing unit [22].

Alternative MAM technologies have the ability to produce parts having similar mechanical properties as L-PBF-produced components [23]. In particular, the application of Bound Metal Deposition (BMD), a metal Fused Filament Fabrication (FFF), is therefore investigated in the present work. This process is an extrusion-based MAM process reliant on a powder-filled thermoplastic medium that, after deposition, is debinded and sintered into solid parts [24]. The machine setup for this process is more straightforward than the L-PBF environment, due to the fact that there is no need for special powder handling or cleaning facilities. The raw material is provided as a solid stock that can be easily handled in a typical workshop space with no additional health requirements and restrictions [25]. One of the primary driving forces of metal FFF compared to L-PBF is the cost of manufacturing that, together with the wide range of available materials and the lack of a powder removal step in the process chain, provides an ideal opportunity to manufacture MAM parts [26]. As the process is inherently different from L-PBF, the application of BMD tools for profile extrusion and especially the interaction between the BMD tool internal surface and the resulting extrudate product surface is unknown and of very high interest.

The work presented in this study directly investigates the capabilities of the BMD metal FFF process and its integration into the tooling process chain for polymer profile extrusion. Through experimental activities, the tooling capabilities of metal FFF components are analyzed and compared with identical conventionally manufactured tool geometries in terms of dimensional tolerances and surface finish that can be obtained. With the successful integration of metal FFF in extrusion tooling, a significant potential due to higher availability of tooling materials, cost savings compared to L-PBF and opportunities to realize optimized extrusion die geometries powered by the design freedom of MAM processes can be clearly exploited.

2 Materials and methods

In this section, the choices made regarding the experimental design and setup will be described. In particular, the following aspects are discussed: the design of the experimental insert split die (Sect. 2.1), the manufacturing of the conventional benchmark inserts (Sect. 2.2), the post-processing considerations for MAM parts (Sect. 2.3), the metrological processes and equipment used for the characterizations of MAM parts (Sect. 2.4) and of extruded products surface (Sects. 2.5), the extrusion experimental setup (Sect. 2.6). A detailed description of the metal FFF process and the manufacturing of the MAM tool inserts is presented separately (Sect. 3).

2.1 Design of the extrusion die with interchangeable insert

In order to allow for an interchangeable experimental setup where several different tooling processes and geometries could be tested while keeping a reduced cost for each setup, an insert-based extrusion die was designed and manufactured. A schematic rendering of the die and corresponding views including insert, polymer flow and sensors are shown in Fig. 1. The die is constructed as a split design, where the cylindrical shape can be separated along its centre axis, and the internal flow channel can be accessed, and then reassembled to perform the extrusion process with the selected interchangeable insert (see Fig. 2). Inside the die, a cavity is present in which a tool insert can be mounted. The design allows the insert to be manufactured using different processes and alterations regarding the geometrical shape of the internal flow channel and the resulting extrudates profile. The die is heated using external ring heaters with temperature controls in the die body. A melt temperature and a pressure sensor are fitted in the flow channel on either side, right before the polymer enters the tool insert (see sensor placement indicated in Fig. 1). These sensors' placement allows monitoring flow changes during experimental variations and future simulation process validation.

The goal of the flow-channel design was to implement a dog-bone–shaped geometry to slow down the central part of the flow, allowing for a balanced flow profile of the polymer upon entering the tool insert channel [27]. The inverse of the flow geometry can be seen in Fig. 3, where the fixed die part and the interchangeable part (i.e. the flow inside the tool insert) are indicated.

2.2 Conventional tool insert manufacturing benchmark

Inserts having the same geometry as described in Sect. 2.1 were first produced by conventional subtractive manufacturing as a benchmark for comparing the MAM tool inserts. The conventional method of manufacturing extrusion dies combines computer numerical control (CNC) milling and electrical discharge machining (EDM). The die inserts are first milled to obtain the primary shape and dimensions of the external sides. Then, the milled die inserts are subjected to EDM for the generation of the internal surfaces, where the polymer melt will flow and will be shaped by the die profile. Thus, the conventional benchmark inserts

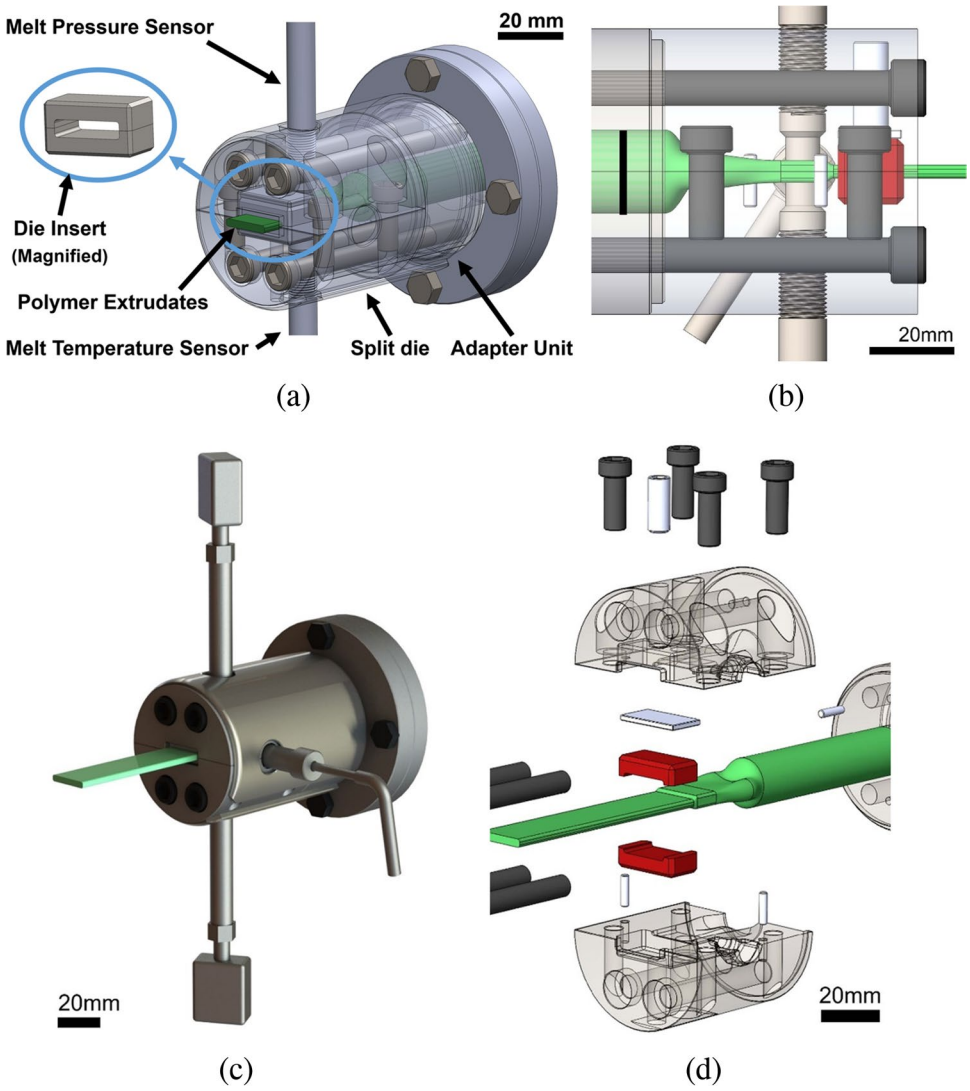

Fig. 1 **a** Schematic rendering of the split die with the placement of the melt sensors and the die insert shown as magnified; **b** side view of the split die; **c** 3D rendering of the split die assembly including extrudates and sensors; **d** exploded view of the split die assembly. Split die overall dimensions: diameter = 68 mm, length = 100 mm

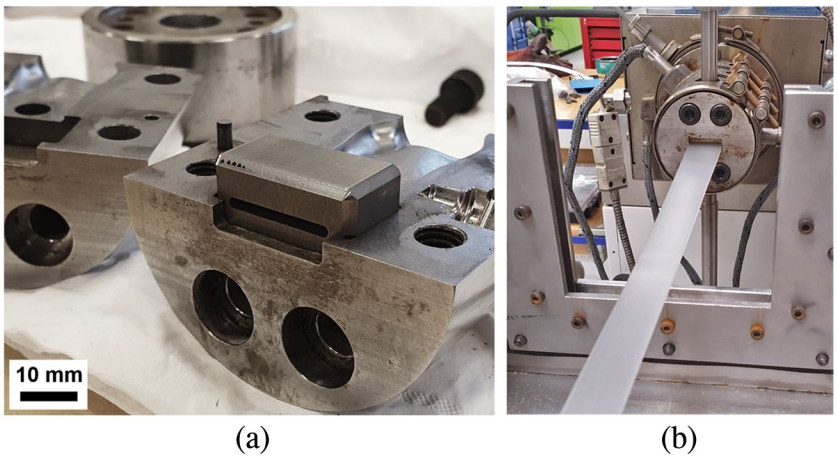

Fig. 2 **a** Manufactured split die in its open state with a conventionally manufactured insert fitted with the upper half and the adapter unit visible in the background; **b** assembled split die with one of the manufactured inserts during the extrusion process

were manufactured using these machining steps, ensuring a close replication of industrial practices. As the primary die surface of interest is solely generated by EDM, the conventional benchmarks are referred to as the EDM parts. The inserts were manufactured with a 1 mm × 20 mm and 2 mm × 20 mm slit geometry, respectively, as shown in

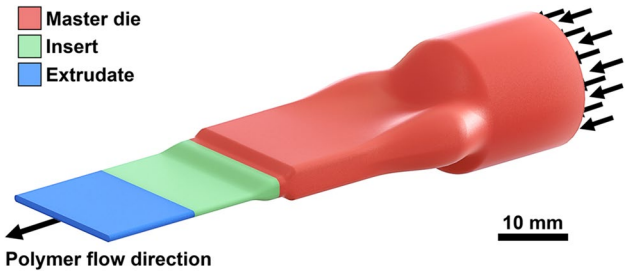

Fig. 3 Inverted die flow channel with indications of the two different flow zones and the final extrudates profile. The flow enters to the right with a cylindrical flow profile and exists to the left as a flat bar

Fig. 4. The specific profile cross section was selected being a standard profile shape in the field of extrusion. Additionally, the high slit-die aspect ratio allows for simulation-driven optimization providing more robust boundary conditions concerning assumptions on the flow development [19, 28]. The tool dies manufactured by conventional machining technologies were produced in EN 1.4404 AISI 316L stainless steel.

As it is an industrial practice in some instances to manufacture tools with a low internal surface roughness for high-quality profiles and selected polymers, two different EDM settings were included for the conventional tool insert benchmarks. Namely arithmetic mean height roughness values targeting $Sa_{fine} \approx 0.2$ µm and $Sa_{coarse} \approx 0.8$ µm. Each of these manufacturing settings will, in the following, be denominated 'EDM – fine' and 'EDM – coarse', respectively. Five tool insert units were manufactured to investigate the manufacturing repeatability of the tooling technologies considered in this study.

2.3 Dimensional and geometrical evaluation

Two different groups of measurands for the tool inserts were selected: the flow outlet channel's dimension and the tool insert's external dimension. For the evaluation of the flow channel exit, an optical coordinate measurement machine (CMM), DeMeet 220 ($U_{DeMeet220} = \pm 4$ µm), based on backlight contrast measurements, was used for the characterization. These dimensions are relevant due to the dimensional requirements of the final extrudates product. A tactile CMM, Zeiss Prismo 5 VAST MPS HTG coordinate measuring machine (E0,MPE = 2,0 + L/300 µm) was used to evaluate the external dimensions of the as-built tool inserts. The CMM was fitted with an Ø3-mm synthetic ruby sphere. The external measurement was conducted using a grid pattern of measurement points to which a plane was fitted, and the inter-plane distances were evaluated and reported.

These dimensions are relevant due to the tool inserts' functional requirements concerning the cavity fitting in the overall die assembly. With improper dimensional accuracy of the tool inserts, it will be impossible to assemble the

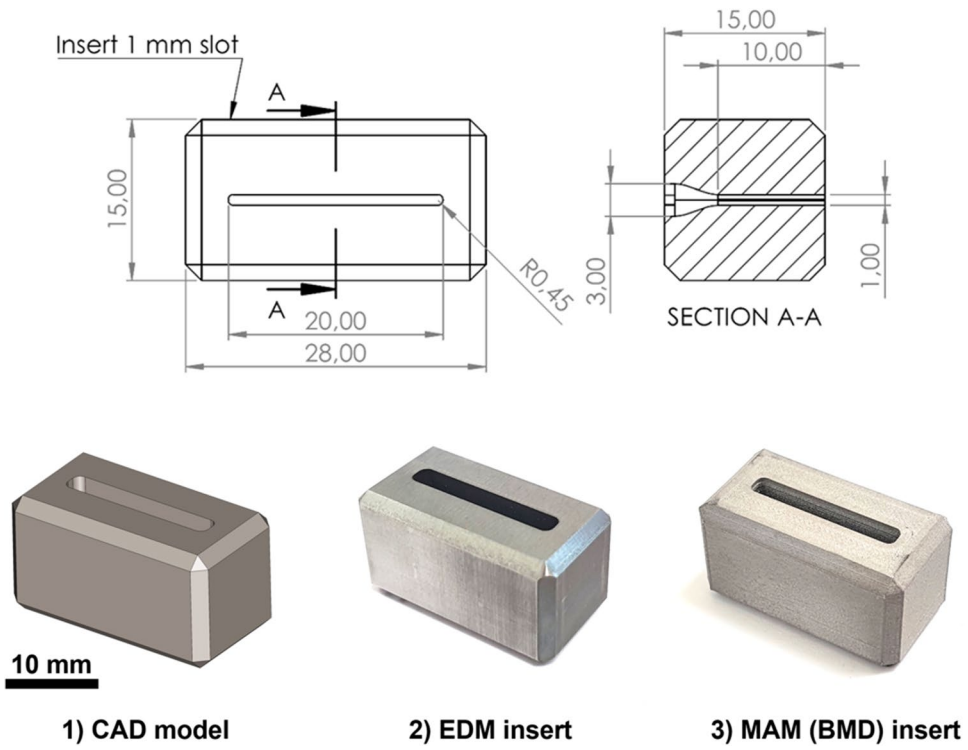

Fig. 4 Top: dimensions of the die tool insert (dimensions in mm). Bottom: examples of the tool insert geometries manufactured using EDM (conventional) and metal FFF process (AM)

die (oversized), or the assembly will be loose, resulting in an overflow of polymer around the insert in the cavity (undersized).

2.4 Surface texture evaluation

For the surface texture evaluation, two different analyses were considered: the internal surface topography of the tool insert and the external surface topography of the resulting extruded product. In order to analyze the internal surface topography, selected inserts were cut in half using EDM in a destructive test, thereby revealing the internal die surface. All surface measurements were acquired using a confocal laser-scanning microscope (CLSM), Olympus Lext 4100, equipped with a × 50 magnification lens.

The acquired surface measurements were subjected to global levelling and global bow removal procedures using Image Metrology Software SPIP. All reported measurands are calculated averages and standard deviations of at least five surface measurements unless otherwise specified. The surface roughness parameters: *Sa*, *Sq*, *S10z*, *Spk* and *Svk* were all determined according to ISO 25178–2:2012 [29].

2.5 Polymer profile extrusion setup

For the polymer extrusion process, a single-screw extruder with a screw diameter of 19.05 mm was used. The main extrusion parameters are listed in Table 1. The extruded polymer was an acrylonitrile butadiene styrene (ABS) resin (INEOS Terluran® HI-10) that had been pre-dried for 2 h at 80 °C prior to extrusion. Following the extruder and the die, the profile was passed through an oversized calibrator disk into a water bath before passing through the pull-off unit. Samples were collected after 5 min of continued extrusion. The extrusion parameters listed in Table 1 were selected in order to allow for a continuous process and a stable production. The extrusion temperature of 195 °C allowed for the required viscosity to achieve a stable melt flow avoiding the risk of polymer degradation. Line production velocity and mass flow were selected to ensure an effective and accurate wind up of the extrudate, and at the same time to optimize productivity.

Table 1 Polymer extrusion process parameters for ABS

Parameter description	Value	Unit
Extrusion temperature	195	°C
Die head pressure	3.8	MPa
Line production velocity	1.3	m/min
Mass flow	32.4	g/min

3 Additive manufacturing of tool inserts

The additive manufacturing of the samples was conducted using the extrusion-based AM method, namely metal FFF. In this process, a feedstock composed by polymeric binder and metallic powder in almost 50%/50% volumetric content is deposited by using a Fused Filament Fabrication approach. Once the so-called green part is formed, the polymer is removed by using a dedicated solvent and thermal debinding processes. While the solvent chemical dissolutes a part of the polymer, the heat (up to almost 600 °C in the thermal debinding step) decomposes the remaining polymer traces. Finally, the voids left by the removed polymer in the part are closed by using sintering densification which consists in the last process step of the process chain.

In this work, a commercial version of metal FFF, called Bound Metal Deposition (BMD) and implemented by Desktop Metal in its Studio System + V1 solution, was adopted to produce the parts. The process imposes three steps after the complete design of the parts: printing, debinding and sintering, all implemented in the system equipment provided by the supplier. The printer of the BMD process has a peculiarity that consist in the presence of two nozzles, the first for the build material and the second one that is aimed at depositing a ceramic-polymer interface material that is used to enable an easy and handy separation of the parts from the supports. The ceramic release layer enables the fabrication of complex parts and assemblies without rigid support structures that are fused to the part. The support and the part can easily be separated, without the need for post-machining the component. The hard particles do not take part in any transformation during the sintering final step. Sintering temperature coagulates the metallic powder without affecting the ceramic state.

For both materials, the polymeric matrix is degraded by the high temperature: the metallic powder undergoes a sintering process, and the ceramic is released from the polymer (namely, it gets pulverized). The result is a metallic component surrounded by ceramic powder; they can be easily separated without the need of post processing.

Stainless steel 17–4 PH (see chemical composition in Table 2), in the form of feedstock Φ6-mm bars as provided by the machine producer, was adopted as build material. This material is a martensitic precipitation-hardened stainless steel used in a wide range of industrial applications including those where tough environments are detected. It is primarily known for its corrosion resistance and high levels of strength and hardness, especially when heat treated.

Table 2 Measured chemical % compositions of the 17–4 PH steel adopted for metal FFF inserts

C	Cr	Ni	Cu	Mn
0.07	15.2	4.1	4.5	1.9

After the insert design, slicing of STL files was conducted using the Desktop Metal proprietary Fabricate software. In this software, all the printing conditions and printing setup were configured. The selected nozzle was the smallest available having 250 µm nominal diameter, in order to maximize the surface resolution on the parts. The two most important printing settings consisting in the Printing Temperature and Printing Speed were set to 15 mm/s and 165 °C, respectively. The build plate temperature was set to 65 °C. A layer height of 0.1 mm was adopted to minimize the staircase effect on the part surfaces.

Given the thickness of the components, which represents a limit for an efficient solvent debindability, the parts were printed by adopting an infill strategy (namely, they were not fully dense in the inner core geometry). A rectilinear grid infill strategy with an infill line distance = 1.75 mm was adopted considering the stringent compression resistance requirement of the die parts under study. The outer portions of the parts, including the inner portions close to the calibrated slot of the dies, were then printed with a shell characterized by a line width = 0.30 mm and a wall line count = 3. The shell is performed by deposition strands aligned with the perimeter and allows to generate regular surface topography. In order to minimize the impact of the fingerprint left on the generated surfaces by the starting and ending deposition points of each layer, these two point coordinates were kept equal among the layers. In this way, a seam aligned vertically and placed at a corner of the parts is generated. Purging intervals after every 30 layers were prescribed on the building material printhead to limit the deviations in the printing behaviour due to the clogging and dirtiness tendency of the printhead.

The parts were printed on a raft base (with extra margins of 3 mm with respect to the part footprint) to foster an even and homogeneous shrinkage of the parts during sintering process, preventing forms of cracking or warping. The raft has sufficient thickness, equal to 1.8 mm, to withstand the warping tendency after debinding and sintering, and is characterized by a density of more than 90% to allow an easier solvent debinding operation.

With these printing parameters, the parts are subjected to a nominal sintering shrinkage of 16% in all the three directions, and therefore, an oversize compensation factor of 19% was adopted accordingly (namely the parts were printed 19% bigger in all directions, with respect to nominal dimensions). With these conditions, the nominal parts' weight in sintered state is 28 g.

Five parts with the same geometry were printed in the same building job. Regarding the parts' orientation during printing, the parts were lying upside down in a horizontal manner (see Fig. 5), with the exiting surface of the die lying in contact with the ceramic interface support material that connects the part with the raft (see Fig. 6). In this way, the entry surface of the die, whose contact connection with the master die is fundamental for the best die coupling, is given the most chance to have optimal quality.

The printing job took around 50 h in total to produce 5 parts altogether. The dewaxing time (i.e. debinding) took

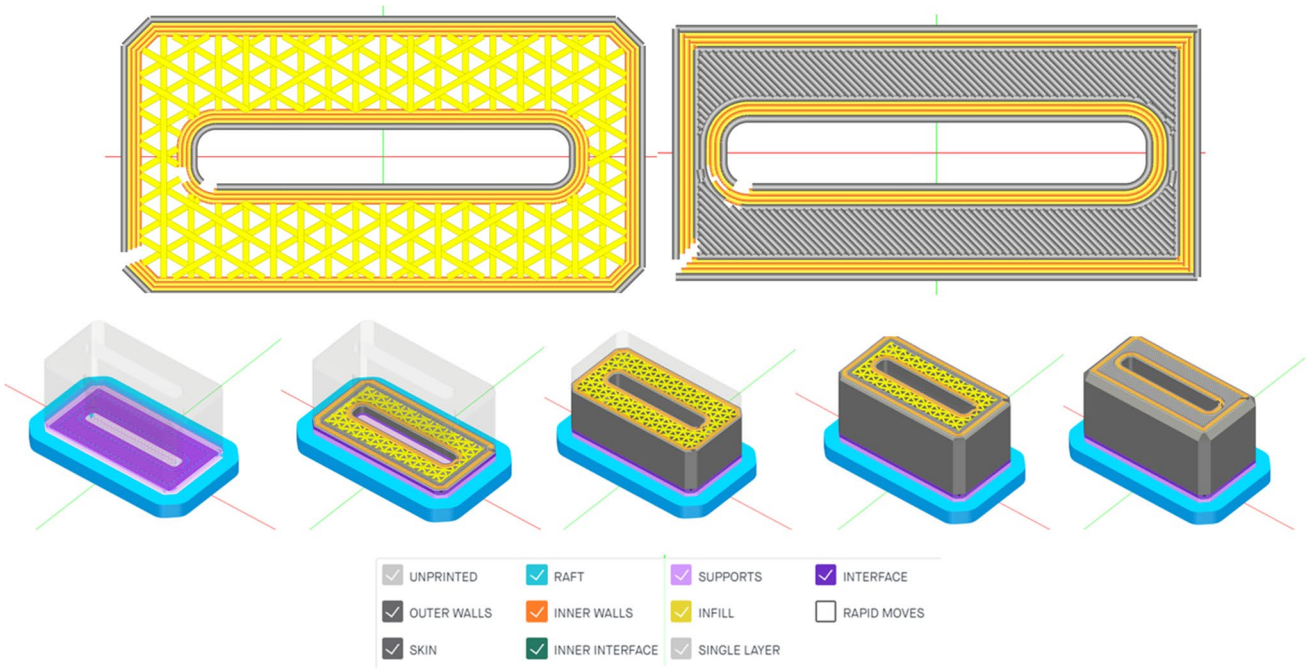

Fig. 5 Sliced part programme for the inserts produced by metal FFF

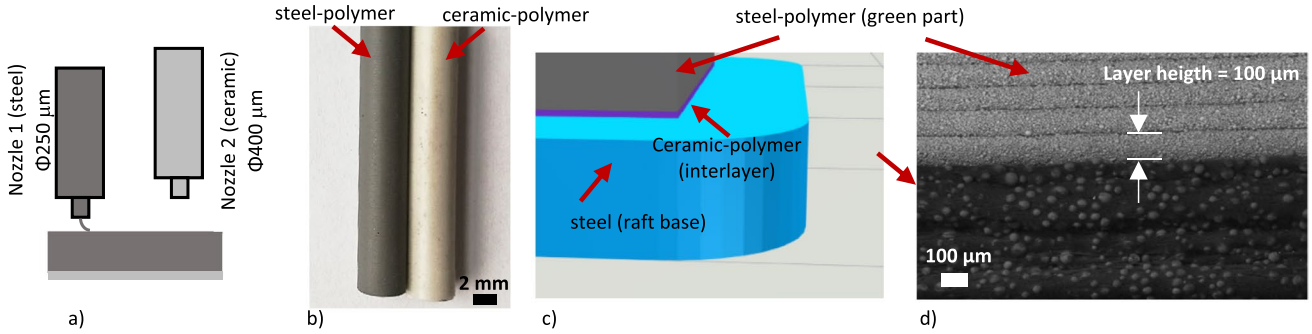

Fig. 6 Raw materials used in the adopted metal FFF system (BMD): **a** two nozzle printing system, **b** metal and ceramic rods, **c** detail of ceramic interlayer deposition, **d** details (scanning electron microscope image) of connection zones between part and raft

around 12 h. Sintering was performed in a gas mixture of argon (97%) and hydrogen (3%) atmosphere at maximum sintering time of 1340 °C for 2 h. The overall sintering cycle required 40 h, including the part cooling (that was performed in the furnace).

A well-known process characteristic of MAM parts is that they contain significant amounts of complex surface features such as pocket holes, inclusions and varying topographies resulting in high surface roughness values that are complicated to quantify [30, 31]. Therefore, utilizing one or more post-processing treatments of AM parts is common practice to achieve usable parts. As several different processes exist dealing with the surface roughness reduction of external surfaces, few processes are successfully capable of significantly treating internal geometries of dimensions below 10 mm [32]. Some studies have shown promising results using hybrid processes, a combination of electrochemical, dynamical abrasive and vibration deburring processes; however, few processes can significantly reduce internal surface roughness [33]. One well-documented process for internal surface treatment is abrasive flow machining. However, it is very cost-intensive and has limitations concerning flow channel geometry, and the abrasive wear is highly dependent on the local surface flow speed [34].

The current study evaluated the manufactured metal FFF tool inserts in an as-built condition. As no previous investigations have been made on the interaction between MAM surfaces and polymer in profile extrusion setups, it is essential to establish a baseline before including different post-processing technologies with questionable results on internal surface topographies. Moreover, the objective of this study was to test the as-built inserts' capability to assess the robustness of the approach on this new process chain. The inclusion of post-processing of metal FFF internal surfaces is discussed further in the section on future investigations.

4 Experimental results

This section describes and discusses the experimental results and findings. First, the printed material is characterized (Sect. 4.1). Then, the manufactured inserts are characterized both from the material point of view and with regard to the dimensional aspects (Sect. 4.2). In particular, the surface topography analysis of the parts is presented and discussed, with a focus on metal FFF inserts (Sect. 4.3) and resulting extrudates surfaces obtained with MAM and conventional dies, respectively (Sect. 4.4). Lastly, polymer flow die interaction considerations are discussed (Sect. 4.5).

4.1 Metal FFF material and process characterization

In order to verify the suitability of the adopted material for the tooling application case under study, a first preliminary characterization campaign was ran. Scanning electron microscope inspection of the green cartridges of 17-4PH confirms that granulometry of the powder adopted for the metal feedstock is characterized by particles that range from about 1 to 20 µm with a very wide distribution (Fig. 7a). Preliminary produced metal FFF sample parts in 17–4 PH printed with a 250-µm nozzle diameter are characterized by internal diffused and regular porosity formation of about 2–5% (with dimension of about 10–50 µm) at green state, Fig. 7b. This characteristic presence of relatively small air voids is typical for all the material extrusion AM and showed a relevant sensitivity with respect to the adopted processing parameters, therefore confirming the importance of the AM extrusion process setup.

The residual porosity in the metal FFF–printed 17–4 PH, Fig. 7b, along with the material microstructure produced in the sintering cycle gives a characteristic

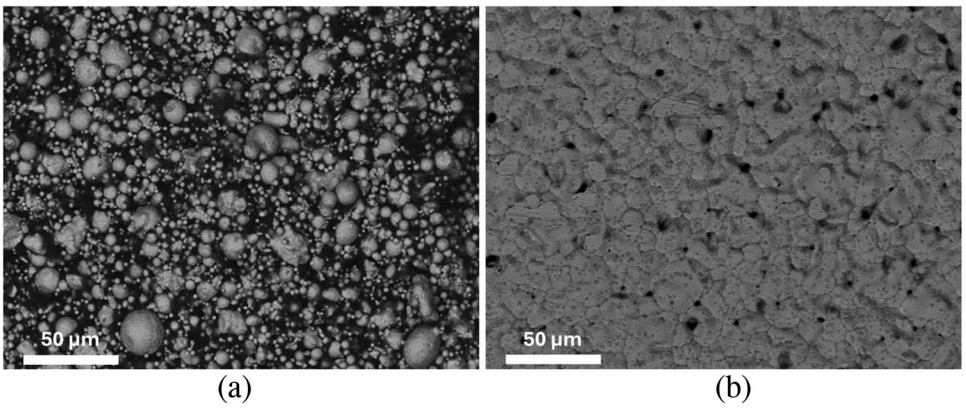

Fig. 7 **a** 17-4PH metal-polymer feedstock adopted for manufacturing the inserts and **b** sintered material surface

Table 3 Measured mechanical properties characteristics of the adopted 17-4PH metal FFF material

Mechanical properties	Value
Yield strength [MPa]	646 ± 14
Ultimate tensile strength [MPa]	833 ± 13
Elongation at break	7.3 ± 1.5
Young Modulus [GPa]	174 ± 12
Hardness [HRC]	23 ± 4

material response from the mechanical point of view that makes the printed material differ from the properties of the wrought material. Since the die inserts under study are subjected to sensible loads both from the mechanical and thermal point of views, a preliminary tensile stress analysis is conducted to characterize mechanical properties. All the tensile tests were performed following the standard ISO 6892–1:2019. Dog-bone specimens with cylindrical geometry (gage length = 30 mm, diameter = 6 mm) and a clip-on extensometer used for axial strain measurements were used. The dog-bone specimens were printed and sintered in horizontal condition by adopting the same printing parameters used for the extrusion inserts. Six replicas were tested to provide the quantification of the test variance. The results listed in Table 3 come from specimens obtained from the adoption of the same printing parameters adopted for printing the inserts. Despite the limited information that the tensile testing can provide with respect to the full list of material requirements given by each application case, the obtained values confirm the suitable material response. The given values are in line with properties produced by metal injection moulding of 17–4 PH [35], and slightly lower than the wrought material [36].

4.2 Metal insert characterizations

The tooling inserts' external dimensions were evaluated (see Table 4) to ensure compatibility in the die tooling setup. The conventionally manufactured tools have a high level of accuracy and are very close to the target dimensions with deviations of the slots dimensions in the range of 0.20–0.50% in the Y direction (1 mm slot height) and 0.02–0.05% in the X direction (20 mm slot width). This is also expected based on the general quality of parts manufactured using precision machining processes such as CNC milling and EDM. Regarding the produced metal FFF inserts, the external dimensional errors in X and Y direction show average amplitudes of − 20 µm and + 70 µm in X and Y direction, respectively, which are about − 0.1% and + 0.3% of the nominal dimensions (i.e. 15 and 28 mm), respectively.

The standard deviation of the deviation errors, obtained by analyzing the different produced insert units, is comparable to the errors' average values indicating a balance between the systematic error component and the random one. The former component can be further compensated by adjusting the STL file oversizing factor while the latter, i.e. the pure process variability, is associated to printing and sintering processes phenomena and cannot be easily controlled.

Interestingly, it can be noted that the green parts are printed systematically smaller than expected (i.e. smaller than the nominal green part size obtained by upscaling the size of the final sintered component). The errors on the green parts size are about 1.1% and 2.5% considering the nominal green parts' sizes of 17.85 mm and 33.32 mm, for X and Y directions, respectively (see 'Dimension X' and 'Dimension Y' of 'Metal FFF—green state' in Table 4), which are obtained by scaling the original STL file to compensate for the shrinkage of 16%. This indicates that the suggested oversizing factors not only account for the sintering shrinkage, but also for some deterministic size errors caused by the printing phase. The average shrinkage happened on each part units results a little larger (of about + 0.6%) in the X direction with respect to Y direction, indicating that there

Table 4 Metal FFF insert dimensions, form and position errors, relative deviation errors and their corresponding repeatability

Sample	Metal FFF—green state	Metal FFF—sintered state
Dimension X (% err)	17.65 ± 0.05 mm (− 1.12 ± 0.26) (*)	14.98 ± 0.03 mm (Nominal dimension = 15.00 mm) (Deviation % error = − 0.08 ± 0.2)
Dimension Y (% err)	32.88 ± 0.04 (-2.45 ± 0.22) (*)	28.07 ± 0.08 (Nominal dimension = 28.00 mm) (Deviation % error = 0.26 ± 0.31)
Perpendicularity + X + Z	0.09 ± 0.01 mm	0.16 ± 0.09 mm
Perpendicularity − X + Z	0.09 ± 0.02 mm	0.12 ± 0.02 mm
Perpendicularity + Y + Z	0.05 ± 0.01 mm	0.15 ± 0.02 mm
Perpendicularity − Y + Z	0.07 ± 0.01 mm	0.17 ± 0.03 mm
Flatness + Z	0.082 ± 0.008 mm	0.086 ± 0.015 mm
Flatness + X	0.083 ± 0.011 mm	0.147 ± 0.076 mm
Flatness − X	0.073 ± 0.014 mm	0.103 ± 0.021 mm
Flatness + Y	0.042 ± 0.006 mm	0.130 ± 0.021 mm
Flatness − Y	0.058 ± 0.009 mm	0.139 ± 0.023 mm
Slot width X—top (% err)	3.52 ± 0.02 mm (− 1.8 ± 0.57)	2.88 ± 0.03 mm (Nominal dimension = 3.00 mm) (Deviation % error = − 4 ± 0.68)
Slot width Y—top (% err)	23.58 ± 0.03 mm (− 0.92 ± 0.14)	19.99 ± 0.01 mm (Nominal dimension = 20.00 mm) (Deviation % error = − 0.05 ± 0.19)
Slot width X—bottom (% err)	/	2.93 ± 0.01 mm (Nominal dimension = 3.00 mm) (Deviation % error = − 2.33 ± 0.25)
Slot width Y—bottom (% err)	/	19.98 ± 0.03 mm (Nominal dimension = 20.00 mm) (Deviation % error = − 0.1 ± 0.35)

(*)Computed with respect to the dimension obtained by including the recommended oversize factors (16%) to take into account for the shrinkage due to the sintering step

is an additional effect of the component shape and material distribution on the final shrinkage.

It must be pointed out that no sensible dimensional deviation is noticed between the green and the debinded parts; therefore, the shrinkage is computed by comparing the green and the sintered dimensions.

The variability of the shrinkage results among the different samples is however very limited (± 0.3%) indicating that the most part of the size errors comes from printing errors and not from a parts' shrinkage response inside the sintering furnace.

In any case, the produced samples are accurate and within the dimensional accuracy limits declared by the metal FFF system provider that are ± 0.5 mm for 17–4 PH material (for lengths up to about 60 mm) despite these values referring to extrusion nozzle with 0.40 mm of diameter (and not 0.25 mm as the one adopted in this study).

Regarding the dimension of the internal slots of the die, relatively high accurate results, within 10 µm of error, are obtained in the Y direction both at the entrance and the exit of the slot. On the shorter dimension, the slot width errors are a little larger (up to 2% on the green parts which become in average 70–120 µm on the sintered parts) probably because of the coupled effects between the discretization issues caused by extrusion nozzle size, the relative larger effect of surface roughness (see Sect. 4.3) and the sintering deformations.

In terms of shape deviations, namely perpendicularity and flatness of the parts external faces, the produced metal FFF inserts present a very high degree of repeatability, suggesting that the BMD is a relatively robust shaping process. Perpendicularity errors of the external vertical part faces with respect to the upper part face, range from about 50–100 µm on the green parts to 120–170 µm on the sintered parts. This underlines the importance of the deformations introduced by the sintering process which are governed by the material distribution and the gravity load effects, as well as the effect of friction between the part and the ceramic setters.

The same considerations can be outlined for the flatness errors of the part faces which appear smaller on the green parts versus the sintered ones. One exception is represented by the vertical face whose flatness error remains unaltered, probably because this surface is the least loaded by the part weight that acts during the sintering as precursor for deformations. The flatness average errors range from 40 to 80 µm on the green parts and 100 to 150 µm on the sintered parts.

As it could be expected, both absolute perpendicularity and flatness errors appear a little smaller on the Y faces (namely, the narrower faces of the mould insert) with respect to X faces (namely, the wider ones), due to their reduced size.

4.3 Metal FFF insert surface topography evaluation

The manufacturing process of the metal FFF method results in very characteristic surface features. Whereas the top surface parallel to the build plane is not so relevant in this study, the side-wall geometry, i.e. perpendicular to the build direction, is of high interest, as this is the surface that constitutes the internal wall of the flow channel in the tool insert. The metal FFF process leaves a rippled surface originating from the layer-by-layer construction of the part, and this topography is preserved in all stages of the metal FFF process, as seen in Fig. 8. As previously described in Sect. 4.2, it can be seen from the figure that the insert in its green state is significantly bigger compared to the debinded (brown) and sintered state due to shrinkage.

The ripple dimension is directly linked to the layer height during the metal FFF process, where the green and the brown parts (as-printed and debinded) have the same dimensions compared to the sintered part that shrinks during the last step. This particular rippled topography is a key fingerprint of the metal FFF process, and its influence on the flow of molten polymer in the extrusion process is one of the main points of interest for this investigation and will be evaluated in the following section.

The surface roughness parameters of the metal FFF surfaces at the different stages in the manufacturing process are presented in Table 5. Despite the dimensional shrinkage happening between the green and brown process step, no significant difference is experienced for the measured roughness parameters in the corresponding states. However, the final sintering of the metal FFF part does introduce an overall increased roughness compared to the green and brown as shown by the increase of the amplitude parameters Sa (arithmetical mean height), *Sq* (root mean square height) and *S10z* (maximum height). A decrease of *Spk* (reduced peak height) from the green, brown and sintered state indicates a

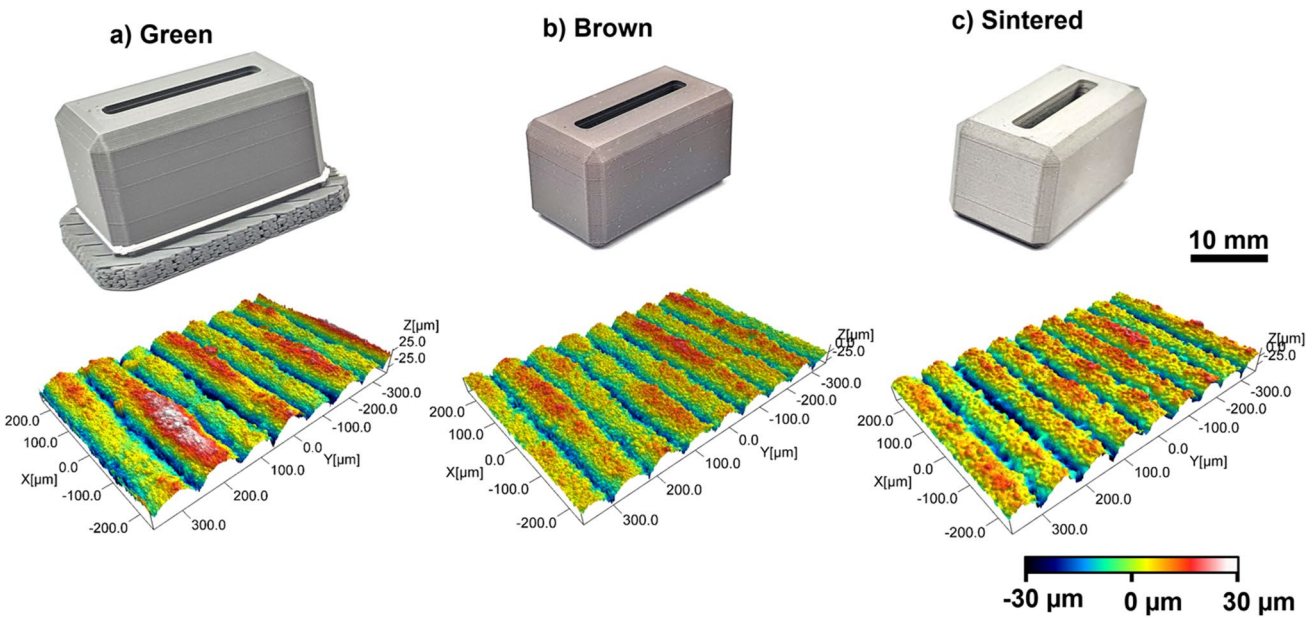

Fig. 8 Internal die cavity surface roughness of MAM tool insert **a** as printed, **b** debinded and **c** sintered. Inserts are shown true to size. Surfaces were measured after cutting the inserts

Table 5 Average surface parameters of internal BMD insert surfaces at different stages of the BMD process. All values reported with standard deviations and are evaluated according to ISO 25178–2:2012 [29]

Sample	Sa [µm]	Sq [µm]	S10z µm]	Spk [µm]	Svk [µm]
Metal FFF—green state	7.8 ± 0.4	9.7 ± 0.5	57.4 ± 3.0	4.9 ± 1.0	15.6 ± 1.2
Metal FFF—brown state	7.4 ± 0.2	9.1 ± 0.3	53.1 ± 2.8	4.6 ± 1.0	12.6 ± 0.5
Metal FFF—sintered state	8.7 ± 0.3	10.6 ± 0.3	61.1 ± 2.0	4.0 ± 0.9	16.7 ± 1.5

decrease of the mean height of peaks above the core surface. An increase of *Svk* (reduced valley depth) from the brown to the sintered state indicates an increase of the mean valley depth below the core roughness. In other words, the sintering process decreases the high of peaks of the surface, and at the same time increases the depth of valleys. This latter phenomenon is dominant, resulting on an overall increase of the amplitude surface parameters, e.g. *Sa*.

4.4 Insert and extrudate surface topography comparison

The internal surface topography of the conventional and the MAM inserts has been compared to evaluate the difference between the as-built metal FFF and two different EDM surfaces. The different surface topographies are shown in Fig. 9. As can be seen from Fig. 8, the insert surfaces originating from the EDM surface and the metal FFF process are very different, with the conventional inserts having the typical EDM surface topography with a more homogeneous distribution of the typical crater-like features. The metal FFF surface has its characteristic ripple topography, as discussed in Sect. 4.2.

The average surface parameters for each of the two inserts groups are shown in Table 6. It can be seen that there is a significant difference between the average surface parameters for the different inserts. This is supported by the clear visual difference shown in Fig. 9. The significant difference in the character of the surfaces is also evident when comparing the surface parameter values as presented in Table 6. The surface of dies produced by metal FFF is clearly higher than those produced by EDM, as indicated by the amplitude parameters *Sa* (2.4–8.7 µm vs. 0.25–0.87 µm), *Sq* (3.0–10.6 µm vs. 0.31–1.11 µm) and *S10z* (20.3–61.1 µm vs. 2.92–11.3 µm). For the surfaces of dies produced by FFF, *Spk* is higher than *Svk*, due to the fact that the mean depth of valleys is larger than the mean height of peaks.

Figure 9 also shows the resulting surface topography of the extruded polymer profile and its corresponding insert. The average surface parameters for the extrudates product are reported in Table 7. The comparison showed a significantly reduced difference in the resulting extrudates' average surface parameters compared to the difference

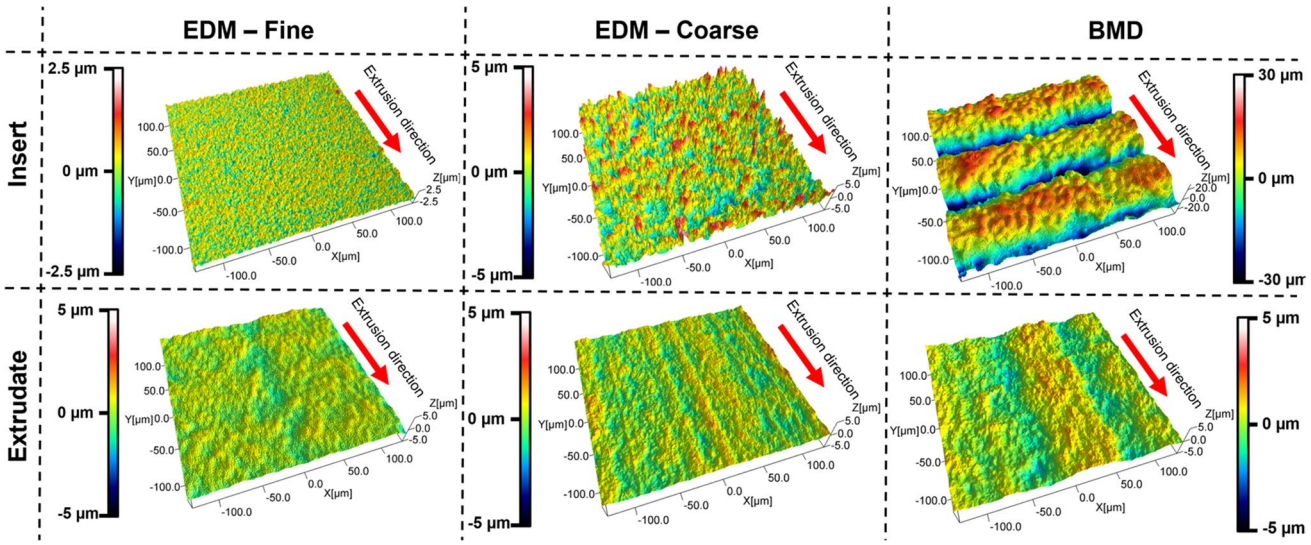

Fig. 9 Internal surface of tool inserts and resulting external surface of polymer extrudates generated by EDM coarse/fine and metal FFF, respectively. Despite the differences in the dimensional scales of the tools, the resulting extrudate surface roughness is of similar amplitude

Table 6 Average surface parameters of internal insert surfaces evaluated according to ISO 25178–2:2012 [29]. All values are averages based on ten measurements and are reported with 1σ standard deviation. (*) See Sect. 4.5

Sample	Sa [µm]	Sq [µm]	S10z [µm]	Spk [µm]	Svk [µm]
Die—EDM fine	0.25 ± 0.01	0.31 ± 0.01	2.92 ± 0.43	0.30 ± 0.03	0.29 ± 0.01
Die—EDM coarse	0.87 ± 0.02	1.11 ± 0.04	11.3 ± 2.3	1.58 ± 0.12	0.73 ± 0.07
Die—metal FFF	8.7 ± 0.3	10.6 ± 0.3	61.1 ± 2.0	4.0 ± 0.9	16.7 ± 1.5
Die—metal FFF (HillTop) (*)	2.4 ± 0.1	3.0 ± 0.2	20.3 ± 2.2	2.8 ± 0.8	3.2 ± 0.4

Table 7 Average surface parameters of extruded product external surfaces. Data is based on 15 measurement points distributed across a sample Sect. (3 by 5 grid) of the manufactured profile. All results reported with 1σ standard deviation

Sample	Sa [µm]	Sq [µm]	S10z [µm]	Spk [µm]	Svk [µm]
Extrudate—EDM fine	0.29 ± 0.08	0.37 ± 0.11	2.45 ± 0.57	0.33 ± 0.16	0.44 ± 0.21
Extrudate—EDM coarse	0.30 ± 0.05	0.38 ± 0.06	2.57 ± 0.37	0.33 ± 0.08	0.39 ± 0.14
Extrudate—metal FFF	0.51 ± 0.10	0.65 ± 0.10	4.81 ± 1.67	0.78 ± 0.32	0.60 ± 0.19

experienced for the tool's internal surface parameters. While the amplitude parameters for the dies produced by metal FFF are in the range of 10–30 times larger than those produced by course and in EDM, respectively, the corresponding surfaces on the plastic extrudates produced by FFF dies have surface roughness that is only 1.8 times higher than those extruded with EDM dies. This means that it is possible to obtain submicrometer surface finish (Sa = 0.51 µm) with an AM die produced by metal FFF, without the need for fine EDM tooling and surface post-processing (i.e. finishing after FFF).

The data presented in Table 7 suggest that there might be a threshold in the extrudate roughness independent of the EDM finishing in the sub-micrometre range. The additional attention towards surface roughness reduction for conventionally manufactured extrusion tools for specific polymers and profiles may be unnecessary as the extrudate roughness is either independent of the tool roughness or has a weak influence on the extrudates when dealing with tool roughness in the sub-micrometre range. The improvement of final extrudate surface roughness may be attributed to other factors in the extrusion matrix, such as calibrator die setup, cooling procedure and extrusion speed, among others, rather than internal tool roughness. Additionally, the influence of melt properties, potential melt fracture and solidification effects may contribute more to the formation of the extrudate surface topography and roughness.

When comparing the surface parameters for the metal FFF inserts, it is noticeable that despite a tool surface roughness of between 5 and 10 times more than that of the EDM tools, the resulting extrudate roughness is only around double that of extrudates by the conventional tools. This again indicates that the correlation between tool surface roughness and resulting extrudate surface roughness may be less significant than other factors. Alternatively, the melt flow interaction with the specific surface topography of the metal FFF tools results in a different interpretation of the tool surface topography by the polymer, as discussed further in Sect. 4.5.

4.5 Flow channel interface discussion

The large discrepancy between the very high difference in roughness values of the tool inserts and the relatively small difference in roughness values of the extrudate products indicates that the mechanism of roughness generation is not significantly affected by the characteristic topography of the metal FFF insert surface. To further enlighten the roughness generation mechanism of the

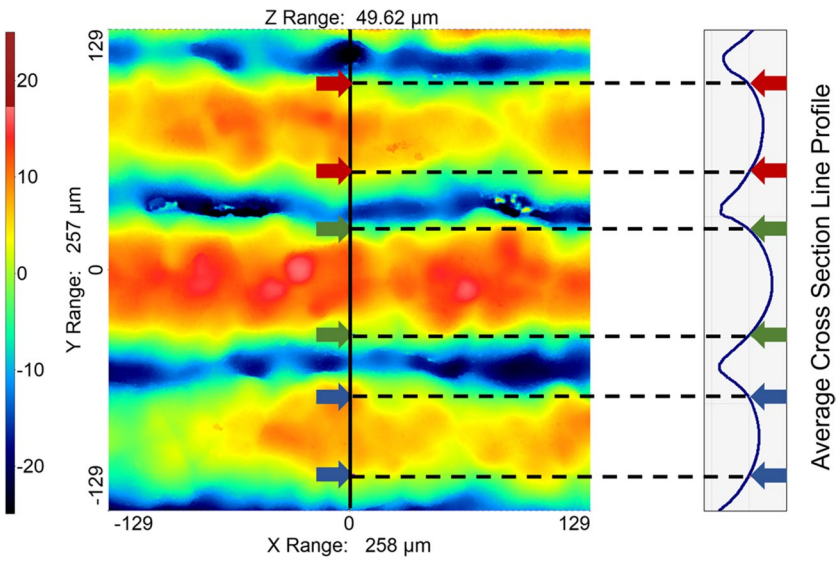

Fig. 10 Identification of cross-section line profile and indications of ridge top inspection area placement shown with arrows. The generated inspection area on the top of each ripple has been evaluated for a region having a width of 20 µm at the intersection between a plane parallel to the XY scanning plane and the scanned surface

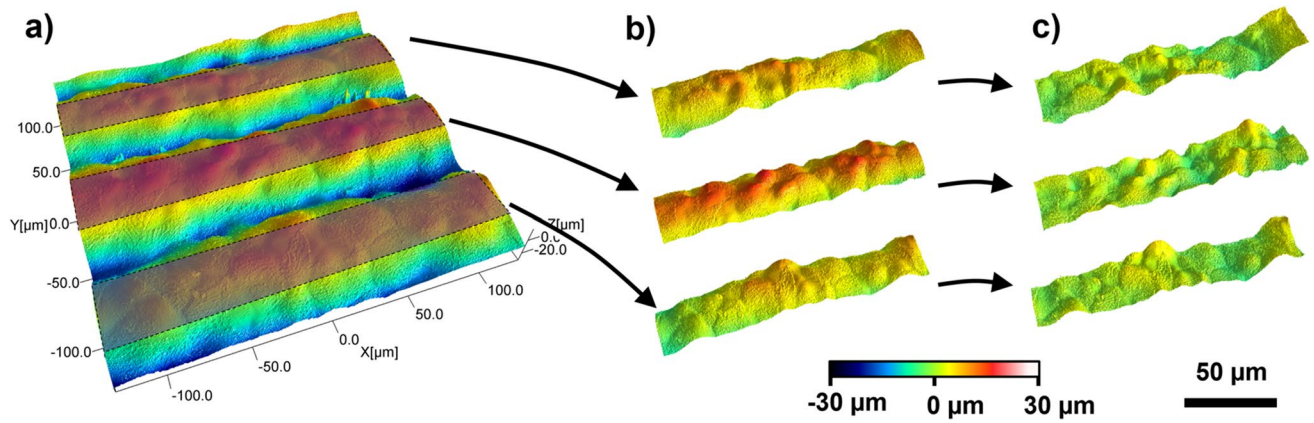

Fig. 11 Surface parameter processing steps: **a** Identify inspection areas of the top ridges on the metal FFF surface. **b** Extraction of surface profile. **c** Global bow removal along the X direction and global levelling of selected inspection area followed by surface parameter evaluation according to ISO 25178–2:2012 [29]

metal FFF surface, additional roughness analysis has been performed. The characteristic nature of the metal FFF surface, with its large ripples, may result in a complex surface interaction. The deep valleys between the high ripples appear to have little to no effect on the high-viscosity polymer flow. Thus, the surface topography of the top of the ridges has been identified and separated from the entirety of the surface, as shown in Fig. 10. These regions are defined as 'HillTop', as indicated in Table 6.

Following the identification of the top ridge, the surface of each ridge has been evaluated following the same methodology as previously described. An example of this process methodology is illustrated in Fig. 11. The resulting surface roughness parameter comparison is reported in Table 7. As it can be seen, this evaluation method significantly filters out the deep valleys of the surface topography in the metal FFF surface. This method may result in a more accurate interpretation of the interaction interface of the internal die polymer flow. The HillTop region of the metal FFF tool surface topography that interacts with the polymeric melt and is mostly responsible in the extrudate surface generation and its corresponding roughness characteristics. Finally, when comparing the effect of the FFF tool roughness parameters, now taking into account the values from the modified evaluation method, it appears that the resulting extrudate average surface roughness values are around twice of those generated by the EDM tools (see Table 7), while the FFF tool *Sa* roughness is 3 to 10 times higher than the course and fine EDM, respectively. This means that a courser tool surface topography does not necessarily generated an accordingly rougher plastic extrudate, suggesting that further surface finishing may not be needed in order to increase the surface quality of extrudated products.

5 Conclusion

The paper presented an implementation of metal FFF for tooling in polymer profile extrusion. The metal FFF process and manufactured tool inserts were characterized, evaluated and compared to conventionally manufactured benchmark tools. The tools were tested experimentally, yielding extrudate samples that were also characterized and compared.

The dimensional evaluation of the additive manufactured tools showed errors up to 150 µm indicating that no tight accuracy can be achieved with this process. The conventional SM tools are instead extremely accurate and repeatable, as it would also be expected for modern EDM and CNC milling. However, it was possible to successfully fit and assemble the die with both sets of inserts.

The resulting external surface parameter variation of the extrudates manufactured using the conventional and the metal FFF tool was significantly reduced compared to the difference experienced on the internal surfaces of the respective tools. This indicates that the internal surface topography of the tool does not entirely determine the resulting surface roughness of the extruded polymer profile. When using dies made by EDM with surface roughness in the sub-micrometre range, no measurable difference was detected on the extrudate surface roughness. The surface roughness parameters of the metal FFF dies may be misleading when evaluated for the entirety of the surface, as the high-viscosity polymer flow is less influenced by the deep valley between two consecutive ripples. Solely evaluating the top of the ripples gives significantly lower roughness parameters, and it better represents the metal FFF surface roughness experienced by the polymer flow.

The implementation of metal FFF has shown that it is possible to apply this MAM process for polymer profile extrusion tooling without subsequent finishing of the as-printed

surface. Compared to conventional tools (where polymer extrudates had an average surface roughness Sa = 0.30 µm), an only slightly increased surface roughness was obtained on extrudates produced with FFF dies (Sa = 0.50 µm). Therefore, depending on the extrudate application, it may be a viable solution.

With this initial confirmation of the successful implementation of metal FFF in the tooling process chain for polymer profile extrusion, it is possible to continue the development of more sophisticated tools for polymer extrusion using metal FFF as tooling technology. Using MAM for tooling in profile extrusion allows for much more complex die designs with optimized internal flow channels that cannot be achieved within the constraints of convention subtractive manufacturing. Through simulation optimization and MAM tooling, balanced dies with lower manufacturing costs and higher throughput may be a reality. In future investigations, it would be interesting to evaluate the influence of post-processing treatments and any possible effects this may have on the quality of the final extrudate.

Author contribution All authors contributed to the study conception and design. Material preparation, data collection and analysis were performed by Martin Kain, Massimiliano Annoni, Paolo Parenti and Guido Tosello. The first draft of the manuscript was written by Martin Kain and Paolo Parenti. All authors commented on previous versions of the manuscript. All authors read and approved the final manuscript.

Funding Open access funding provided by Technical University of Denmark. The work presented in this article has received funding by Marie M.B. Richters Fond (Denmark) (project no. 17–11014) and Politecnico di Milano (Italy). In particular, for this latter, the Italian Ministry of Education, University and Research, is acknowledged for the support provided through the project 'Department of Excellence LIS4.0—Lightweight and Smart Structures for Industry 4.0'.

Declarations

Competing Interests The authors declare no competing interests.

References

1. Wohlers Report (2022) 3D printing and additive manufacturing global state of the industry. Wohlers Associations 2022 ASTM International, p 425. https://wohlersassociates.com/product/wohlers-report-2022/
2. Chua CK, Leong KF, Liu ZH (2015) Rapid tooling in manufacturing; In: Handbook of manufacturing engineering and technology (1st ed) London 1: Springer
3. Hällgren S, Pejryd L, Ekengren J (2016) Additive manufacturing and high speed machining - cost comparison of short lead time manufacturing methods. J Procedia CIRP 50:384–389
4. Atzeni E, Iuliano L, Marchiandi G, Minetola P, Salmi A, Bassoli E, Denti L, Gatto A (2014) In: High Value Manufacturing by Bártolo et al. 2014. CRC Press - Taylor & Francis Group, London, pp 3–8. https://doi.org/10.1201/b15961-3
5. Sossou G, Demoly F, Gomes S, Montavon G (2022) An assembly-oriented design framework for additive manufacturing. Designs 6(1). 1https://doi.org/10.3390/designs6010020
6. Iqbal A, Zhao G, Suhaimi H, He N, Hussain G, Zhao W (n.d.) Readiness of subtractive and additive manufacturing and their sustainable amalgamation from the perspective of Industry 4.0: a comprehensive review. https://doi.org/10.1007/s00170-020-06287-6/Published
7. Gries S, Meyer G, Wonisch A, Jakobi R, Mittelstedt C (2021) Towards enhancing the potential of injection molding tools through optimized close-contour cooling and additive manufacturing. Mater 14(12). https://doi.org/10.3390/ma14123434
8. Vasco J, Barreiros FM, Nabais A, Reis N (2019) Additive manufacturing applied to injection moulding: technical and economic impact. Rapid Prototyp J 25(7):1241–1249. https://doi.org/10.1108/RPJ-07-2018-0179
9. Homar D, Čerče L, Kopač J (2017) Cooling simulation of conformal cooling injection mould insert produced by hybrid manufacturing. Tehnicki Vjesnik - Technical Gazette 24(4). https://doi.org/10.17559/tv-20150909075338
10. Hölker R, Jäger A, Ben Khalifa N, Tekkaya AE (2013) Controlling heat balance in hot aluminum extrusion by additive manufactured extrusion dies with conformal cooling channels. Int J Precis Eng Manuf 14(8):1487–1493. https://doi.org/10.1007/s12541-013-0200-1
11. Hölker R, Haase M, Ben Khalifa N, Tekkaya AE (2014) Increased productivity in hot aluminum extrusion by using extrusion dies with inner cooling channels manufactured by rapid tooling. Key Eng Mater 611–612:981–988. https://doi.org/10.4028/www.scientific.net/KEM.611-612.981
12. Hölker R, Tekkaya AE (2016) Advancements in the manufacturing of dies for hot aluminum extrusion with conformal cooling channels. Int J Adv Manuf Technol 83(5–8):1209–1220. https://doi.org/10.1007/s00170-015-7647-4
13. Munot A, Mead JL, Orroth SA, Stacer RG (1999) Use of stereolithography for extrusion dies. In: Proceedings of the 1999 Annual Technical Conference (ANTEC) of the Society of Plastics Engineers (SPE) pp 58–62
14. Yesildag N, Hopmann C, Windeck C, Bremen S, Wissenbach K, Merkt S (2017) Opportunities and challenges of profile extrusion dies produced by additive manufacturing processes. AIP Conf Proc 1914:04002. https://doi.org/10.1063/1.5016712
15. Kain M, Calaon M, Pedersen DB, Tosello G (2020) On the implementation of metal additive manufacturing in the tooling process chain for polymer profile extrusion. Procedia CIRP 93:26–31. https://doi.org/10.1016/j.procir.2020.03.141
16. Peng X, Kong L, Fuh JYH, Wang H (2021) A review of post-processing technologies in additive manufacturing. J Manuf Process 5(2). MDPI AG. https://doi.org/10.3390/jmmp5020038
17. Marin F, Fagali De Souza A, Ahrens CH, Luis LD, Lacalle N (2021) A new hybrid process combining machining and selective laser melting to manufacture an advanced concept of conformal cooling channels for plastic injection molds. Int J

Adv Manuf Technol 113:1561–1576. https://doi.org/10.1007/s00170-021-06720-4/Published
18. Chan YL, Diegel O, Xu X (2021) A machined substrate hybrid additive manufacturing strategy for injection moulding inserts. Int J Adv Manuf Technol 112(1–2):577–588. https://doi.org/10.1007/s00170-020-06366-8
19. Mackley MR, Rutgers RPG, Gilbert DG (1998) Surface instabilities during the extrusion of linear low density polyethylene. J Nonnewton Fluid Mech 76:281–297. https://doi.org/10.1016/S0377-0257(97)00122-5
20. Arda DR, Mackley MR (2005) The effect of die exit curvature, die surface roughness and a fluoropolymer additive on sharkskin extrusion instabilities in polyethylene processing. J Nonnewton Fluid Mech 126:47–61. https://doi.org/10.1016/j.jnnfm.2004.12.005
21. Calderaro DR, Lacerda DP, Veit DR (2020) Selection of additive manufacturing technologies in productive systems: a decision support model. Gestao e Producao 27(3). https://doi.org/10.1590/0104-530x5363-20
22. Bours J, Adzima B, Gladwin S, Cabral J, Mau S (2017) Addressing hazardous implications of additive manufacturing: complementing life cycle assessment with a framework for evaluating direct human health and environmental impacts. J Ind Ecol 21:S25–S36. https://doi.org/10.1111/jiec.12587
23. Lavecchia F, Pellegrini A, Galantucci LM (2022) Comparative study on the properties of 17–4 PH stainless steel parts made by metal fused filament fabrication process and atomic diffusion additive manufacturing. Rapid Prototyp J. https://doi.org/10.1108/RPJ-12-2021-0350
24. Caminero MÁ, Romero A, Chacón JM, Núñez PJ, García-Plaza E, Rodríguez GP (2021) Additive manufacturing of 316L stainless-steel structures using fused filament fabrication technology: mechanical and geometric properties. Rapid Prototyp J 27(3):583–591. https://doi.org/10.1108/RPJ-06-2020-0120
25. Parenti P, Puccio D, Colosimo BM, Semeraro Q (2022) A new solution for assessing the printability of 17–4 PH gyroids produced via extrusion-based metal AM. J Manuf Proc 74:557–572. https://doi.org/10.1016/j.jmapro.2021.12.043
26. Parenti P, Puccio D, Semeraro Q, Colosimo BM (2023) A techno-economic approach for decision-making in metal additive manufacturing: metal extrusion versus single and multiple laser powder bed fusion. Prog Addit Manuf pp 1–26. https://doi.org/10.1007/s40964-023-00442-7
27. Hopmann C, Michaeli W (2016) Extrusion dies for plastics and rubber, 4th edn. Hanser Publications, Munich
28. Zitzenbacher G, Brunner E (2019) Evaluation of the influence of the tool surface on polymer melt flow using a novel rheological extrusion slit die. AIP Conf Proc 2055:040001. https://doi.org/10.1063/1.5084816
29. Standard E (2012) Geometrical product specifications (GPS) – surface texture: areal – part 2: terms, definitions and surface texture parameters, EN ISO 25178–2:2012. European Committee for Standardization, Brussels
30. Leach RK, Bourell D, Carmignato S, Donmez A, Senin N, Dewulf W (2019) Geometrical metrology for metal additive manufacturing. CIRP Ann 68(2):677–700. https://doi.org/10.1016/j.cirp.2019.05.004
31. Thompson A, Senin N, Maskery I, Körner L, Lawes S, Leach R (2018) Internal surface measurement of metal powder bed fusion parts. Addit Manuf 20:126–133. https://doi.org/10.1016/j.addma.2018.01.003
32. Nagalingam AP, Yeo SH (2020) Surface finishing of additively manufactured Inconel 625 complex internal channels: a case study using a multi-jet hydrodynamic approach. Addit Manuf 36. https://doi.org/10.1016/j.addma.2020.101428
33. Duval-Chaneac MS, Han S, Claudin C, Salvatore F, Bajolet J, Rech J (2018) Experimental study on finishing of internal laser melting (SLM) surface with abrasive flow machining (AFM). Precis Eng 54:1–6. https://doi.org/10.1016/j.precisioneng.2018.03.006
34. Wahab Hashmi A, Singh Mali H, Meena A (2022) Experimental investigation on abrasive flow Machining (AFM) of FDM printed hollow truncated cone parts. Materials Today: Proceedings 56:1369–1375. https://doi.org/10.1016/j.matpr.2021.11.428
35. Machaka R (2018) Metal injection moulding of a 17–4 PH stainless steel: a comparative study of mechanical properties. IOP Conf Ser: Mater Sci Eng 430:012033. https://doi.org/10.1088/1757-899X/430/1/012033
36. Gruppo Lucefin (2012) Precipitation hardening stainless steel X5CrNiCuNb6-4 1.4542. Available at: http://www.lucefin.com/wp-content/files_mf/1.4542pha63062.pdf. Accessed 29 Mar 2024